Extracellular vesicles of stromal origin target and support hematopoietic stem and progenitor cells

Gregoire Stik, Simon Crequit, Laurence Petit, Jennifer Durant, Pierre Charbord, Thierry Jaffredo,* and Charles Durand*

Sorbonne Universités, University Pierre et Marie Curie Paris 06, Centre National de la Recherche Scientifique 7622, Institut National de la Santé et de la Recherche Médicale U 1156, Institute de Biologie Paris Siene, Laboratoire de Biologie du Développement, Paris, France

Extracellular vesicles (EVs) have been recently reported as crucial mediators in cell-to-cell communication in development and disease. In this study, we investigate whether mesenchymal stromal cells that constitute a supportive microenvironment for hematopoietic stem and progenitor cells (HSPCs) released EVs that could affect the gene expression and function of HSPCs. By taking advantage of two fetal liver–derived stromal lines with widely differing abilities to maintain HSPCs ex vivo, we demonstrate that stromal EVs play a critical role in the regulation of HSPCs. Both supportive and nonsupportive stromal lines secreted EVs, but only those delivered by the supportive line were taken up by HSPCs ex vivo and in vivo. These EVs harbored a specific molecular signature, modulated the gene expression in HSPCs after uptake, and maintained the survival and clonogenic potential of HSPCs, presumably by preventing apoptosis. In conclusion, our study reveals that EVs are an important component of the HSPC niche, which may have major applications in regenerative medicine.

Introduction

Extracellular vesicles (EVs) are emerging as new crucial mediators of cell-to-cell communication (Simons and Raposo, 2009). These heterogeneous nano-sized EVs (30–130 nm) originate from multivesicular bodies (MVBs), which themselves result from inward budding of the membrane of late endosomes. EVs are released by many types of cells in both normal and pathological conditions, including tumor cells, immune cells, and mesenchymal cells (Colombo et al., 2014). EVs are liberated in the extracellular environment after fusion of the MVB with the plasma membrane and can either target cells localized in the microenvironment or be carried to distant sites via biological fluids. They display particular protein and lipid signatures and harbor a specific nucleic acid content with various RNA species having regulatory functions, including miRNAs, tRNAs, ribosomal RNAs, and long noncoding RNAs (lncRNAs; Nolte-'t Hoen et al., 2012; Baglio et al., 2015; Pefanis et al., 2015).

The first evidence of the transfer of functional RNAs from EVs to recipients was shown in mast cells (Valadi et al., 2007). Since then, many studies have described the role of EV RNAs taken up by recipient cells in cancer development, immune response, and cell reprogramming (Mittelbrunn et al., 2011; Hoshino et al., 2015; Quesenberry et al., 2015). Regarding the hematopoietic system, the transfer of exosomal mRNAs and proteins from embryonic stem cells to hematopoietic stem and progenitor cells (HSPCs) has been shown to induce their partial reprograming (Ratajczak et al., 2006). More recently, mRNAs and miRNAs derived from mast cell EVs have been shown to be transferred to human blood $CD34^+$ progenitors, raising the possibility that hematopoiesis is partially controlled by EVs (Ekström et al., 2012).

HSPCs, responsible for the lifelong maintenance and regeneration of the adult blood system, function in close association with a supportive microenvironment (or niche) primarily made of mesenchymal stromal/stem cells (MSCs; Abkowitz et al., 1995; Charbord, 2010; Morrison and Scadden, 2014). The establishment of stromal lines from various hematopoietic tissues, including the fetal liver (FL) and bone marrow (BM), has been instrumental for studying the roles of the hematopoietic microenvironment ex vivo. Experimentally, stromal cells are cocultured with HSPCs, and appropriate in vitro and in vivo assays are used to examine their capability to support HSPCs (Moore et al., 1997; Oostendorp et al., 2005; Chateauvieux et al., 2007). Moreover, stromal lines also constitute an exceptional tool for identifying novel HSPC regulators (Hackney et al., 2002; Oostendorp et al., 2005; Durand et al., 2007; Charbord et al., 2014). Stromal cells are thought to operate on HSPC functions through

*T. Jaffredo and C. Durand contributed equally to this paper.

Correspondence to Charles Durand: charles.durand@upmc.fr; Pierre Charbord: pierre.charbord@inserm.fr

G. Stik's present address is Centre for Genomic Regulation, Parque Investigación Biomédica Barcelona, Barcelona, Spain.

Abbreviations used: APC, allophycocyanin; BM, bone marrow; CM, conditioned medium; DEG, differentially expressed gene; EV, extracellular vesicle; FL, fetal liver; GO, gene ontology; HSPC, hematopoietic stem and progenitor cell; IPA, ingenuity pathway analysis; KD, knockdown; lncRNA, long noncoding RNA; MSC, mesenchymal stromal/stem cell; MVB, multivesicular body; PCA, principal component analysis; PE, phycoerythrin; RPKM, reads per kilobase per million mapped reads.

The Rockefeller University Press
J. Cell Biol. Vol. 216 No. 7 2217–2230
https://doi.org/10.1083/jcb.201601109

cell adhesion, cell-to-cell communication, and extracellular matrix remodeling. Using a systems biology approach based on the comparison of the transcriptomes of several stromal lines of different origins, we recently identified a molecular core representative and predictive of the HSPC support (Charbord et al., 2014). However, the method by which stromal cells exert their biological functions to HSPCs is not fully understood. It certainly includes the aforementioned classical ligand-to-receptor interactions, but the recent discovery that stromal cells release biologically active EVs (Bruno et al., 2009) raises the exciting possibility that EVs may be an additional novel process through which stromal cells carry out their function upon HSPCs.

This study aims at assessing the existence and functionality of stromal cell–derived EVs and their role in the HSPC support. To address this issue, we used two murine stromal cell lines derived from the mouse FL with widely differing abilities to maintain human and mouse HSPCs ex vivo (Moore et al., 1997; Hackney et al., 2002; Nolta et al., 2002; Charbord et al., 2014). We demonstrate that, whereas both stromal lines release EVs, HSPCs specifically take up those produced by the supportive stromal line. These EVs maintain HSPC survival and clonogenic potential in vitro by preventing them from entering apoptosis. Transcriptomic analyses show that EVs released by the supportive stromal line harbor a specific molecular signature and modify the expression profile of HSPCs after uptake. These findings reveal that EVs constitute an important and novel cargo of molecules mediating the HSPC-supporting capacity of stromal cells. Our unprecedented effort to resolve the molecular complexity of HSPC-targeted EVs may help designing innovative stromal-free culture conditions to deliver specific molecules to HSPCs.

Results

Both AFT024 (AFT) and BFC012 (BFC) stromal lines release bona fide EVs

To uncover the presence of stromal cell–derived EVs and analyze their functionality on HSPC support, we used two murine FL stromal lines with contrasted capacities to maintain HSPCs ex vivo. AFT024 displays a potent HSPC-supporting capacity ex vivo, as revealed by long-term cultures and in vivo repopulation assays, whereas BFC012 is nonsupportive (Hackney et al., 2002; Charbord et al., 2014). Transmission electron microscopy revealed the presence of numerous MVBs in the cytoplasm of both cell lines (Fig. 1, A and C). At high magnification, these MVBs contained smaller vesicles of EV size (Fig. 1, B and D). In some instances, we captured the release of EVs outside the stromal cells, likely resulting from the MVB fusion with the plasma membrane (Fig. 1 E). To precisely characterize the type of EV, the extracellular vesicular fractions from both cell lines were isolated from culture supernatants by centrifugation, microfiltration, and ultracentrifugation steps (Théry et al., 2006) and submitted to an ensemble of investigations (e.g., cryo transmission electron microscopy [cryoTEM], flow cytometry, nucleic acid, and protein analyses). CryoTEM analysis of the vesicular fraction from both cell lines revealed round microvesicular structures sized 30–110 nm with an external lipid bilayer characteristic of EVs (Fig. 1, F–I). Electron micrography revealed slightly larger sizes for AFT-derived EVs (AFT EVs) compared with BFC-derived EVs (BFC EVs) but a similar amount of total protein in the EV fraction, revealing similar amounts of EVs released by both stromal lines (Fig. 1, J and K). To further identify AFT EVs versus BFC EVs, we used a novel high-resolution flow cytometry–based method recently developed for quantitative high throughput analysis of individual immune-labeled nano-sized vesicles (van der Vlist et al., 2012). Flow cytometry disclosed the expression of CD63 and CD9, two members of the tetraspanin family known to be hallmarks of EVs. We found that 94.4% of AFT EVs and 88.5% of BFC EVs expressed CD63 (Fig. 1 L). For both cell lines, two EV populations were detected based on the expression levels of CD63, and back-gating analysis of these populations revealed distinct forward and side-scatter light values, suggesting differences of refractive index, shape, or granularity (Figs. 1 L and S1, A–C). CD9 was detected on 92.4 and 63.3% of AFT and BFC EVs, respectively, but was expressed at higher levels in AFT EVs compared with BFC EVs (Figs. 1 L and S1, A–C). Interestingly, the differential expression levels of CD9 between AFT and BFC was observed for EVs but not for whole cells (Fig. S1, D and E). Finally, <5% of the AFT and BFC EVs were positive for annexin V, excluding contamination by bigger microparticles (Fig. S1 B). Western blot analysis of the AFT EV fraction confirmed CD9 expression and allowed the detection of LAMP1 and TSG101, two additional markers of EVs (Fig. 1 M). Finally, analysis of the RNA species revealed the enrichment of small RNAs and the lack of 18S and 28S RNAs in the EV fractions compared with the cells of origin (Fig. 1 N). Collectively, converging evidence indicate that both stromal lines release bona fide nano-sized EVs, the supportive cell line producing EVs that exhibit an enriched surface expression of CD9 compared with its nonsupportive counterpart.

AFT EVs are taken up by HSPCs

We first investigated whether stromal EVs could be taken up by BM cells in bulk culture. BM cells were cultured for 24 h in the presence of two doses of AFT or BFC EVs stained with PKH67 (Fig. S2). Low to nil uptake was observed for the nonhematopoietic CD45-negative cell fraction. In contrast, $CD45^+$ cells indifferently took up AFT and BFC EVs, albeit at low levels. Interestingly, with the higher dose of EVs, we observed a preferential uptake of AFT EVs by Lin^- $Sca1^+$ $c\text{-}kit^+$ (LSK) HSPCs (Fig. S2, A and B). To further examine the tropism of EVs for HSPCs, LSK cells were sorted and cultured with purified stromal EVs stained with PKH67. We observed that LSK cells preferentially internalized AFT EVs in comparison with BFC ones (32.4 and 3.9%, respectively; Fig. 2 A). ImageStreamX analysis that allows quantitative detection of molecule internalization clearly showed that AFT EVs were clustered within LSK cells, contrasting with the weakness and membrane staining observed with BFC EVs (Fig. 2 B). To further validate the specific uptake of AFT EVs by LSK cells, we constructed an AFT stromal line stably expressing a CD63-tagged GFP protein and cocultured these cells with LSK for 96 h (Fig. 2 C). ImageStreamX analysis of the cocultures showed that ∼20% of the $CD45^+$ hematopoietic cells were GFP^+, indicating a direct transfer of AFT EVs to LSK cells (Fig. 2, D and E). Finally, the in vivo uptake of AFT EVs was investigated by intrafemoral injection of stained EVs. Although flow cytometry revealed a low amount of EV internalization in $CD45^-$ cells, internalization was pronounced in $CD45^+$ cells and was found preferentially in LSK cells (Fig. 2 F) in keeping with the in vitro bulk culture. Collectively, these complementary approaches strongly support the finding that AFT EVs specifically target LSK cells.

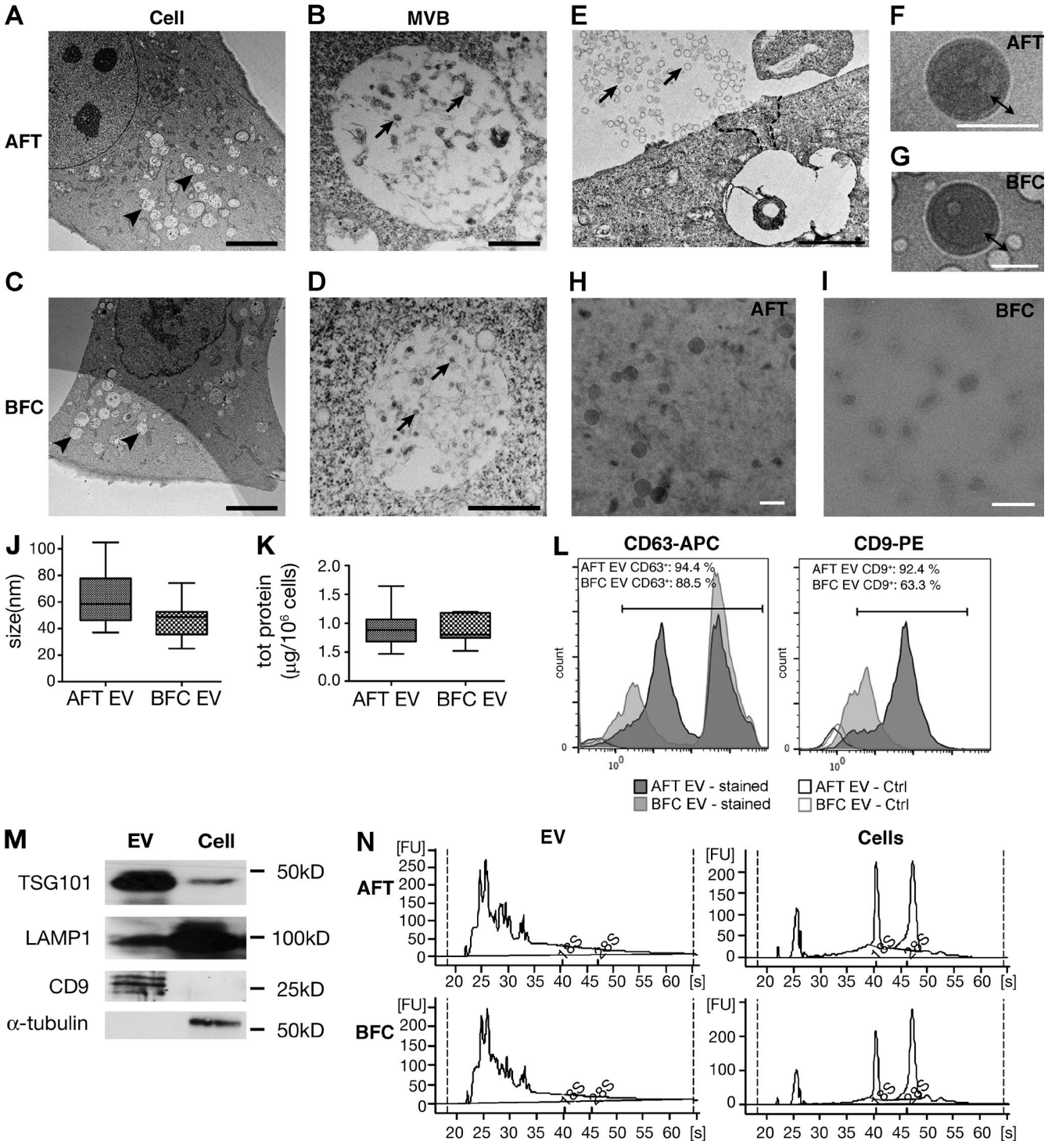

Figure 1. **Characterization of AFT- and BFC-released EVs.** (A–I) Electron microscopy characterization. (A and C) AFT (A) and BFC (C) cell lines showing MVB structures (arrowheads) in the cell cytoplasm. (B) MVB magnification of AFT MVBs showing round structures (arrows) of EV size. (D) Same as B, but with BFC. (E) AFT cell releasing EVs (arrows). The dotted line depicts the connection between the MVB and the cell surface. (F) AFT EV observed by cryoTEM. (G) BFC EV observed by cryoTEM. Double-headed arrows indicate the external lipid bilayer. (H and I) AFT EV (H) and BFC EV (I) observed at a larger scale. Bars: (A and C) 5 µm; (B and D) 500 nm; (E) 2 µm; (F–I) 50 nm. (J and K) Size measurement (J) and total protein quantification (K) of AFT and BFC EVs. (L) Flow cytometric analysis of CD63 (left) and CD9 (right) expression on the EV fraction from AFT and BFC cell culture medium. Box and whisker plots describe interquartile ranges and SD. Tot, total. (M) Western blot analysis of TSG101, LAMP1, CD9, and α-tubulin expression in AFT EVs and cells. (N) Bioanalyzer sizing and quantification of AFT and BFC RNA from EVs and cells. FU, fluorescent unit.

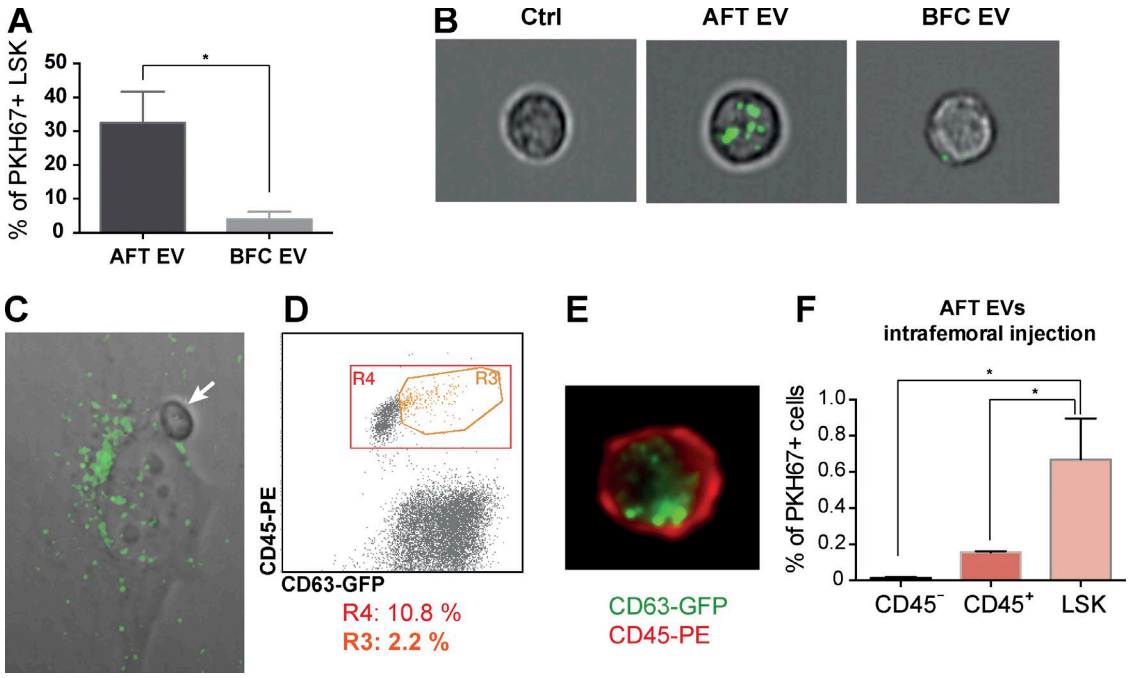

Figure 2. **Internalization of AFT- and BFC-derived EVs.** (A) Quantification of AFT and BFC EV internalization by LSK cells analyzed by ImageStreamX (Amnis; $n = 3$). (B) Representative micrographs of LSK cells. Green dots show PKH67-stained EVs (600× magnification). (C) AFT cell expressing CD63-GFP in close contact with a hematopoietic cell (white arrow; 400× magnification). (D) Coculture of AFT-CD63-GFP with LSK cells. ImageStreamX analysis with GFP and CD45 expression. The hematopoietic cell population is contained within the red-framed area R4. R3 represents CD45$^+$ GFP$^+$ double-positive cells. Percentages are indicated below the graph. (E) Cell representative of R3. (F) Internalization of AFT EV by CD45$^-$, CD45$^+$, and LSK cells 24 h after intrafemoral injection. Error bars show SEM. *, $P < 0.05$.

Ex vivo HSPC maintenance capacity of AFT EVs

We evaluated the effect of stromal cell–derived EVs on cell growth, clonogenic hematopoietic potential, and LSK phenotype. LSK cells were cocultured for 96 h with two doses of EVs in the absence of cytokines. We observed a seven- and 15-fold significant increase ($P < 0.05$) in hematopoietic cell number when LSK cells were cocultured with 20 µg and 60 µg of AFT EV, respectively, as compared with control (LSK alone; Fig. 3 A). In sharp contrast, the number of hematopoietic cells remained unchanged when LSK cells were cocultured with BFC EVs (Fig. 3 A). AFT EVs also maintained the clonogenic potential of LSK cells because a 3.9- and a fivefold significant ($P < 0.05$) increase in colony-forming units were observed after coculturing with 20 and 60 µg of AFT EVs, respectively (Fig. 3, B and C), whereas BFC EVs had no effect. AFT EVs also displayed a supportive effect on LSK cells because a significantly ($P < 0.05$) higher number (3.5-fold) of LSK cells were maintained in culture compared with control despite a global decrease of LSK cells at 96 h from culture incipience (Fig. 3 D). To support this observation, we analyzed whether a decrease in the release of EVs could impact HSPC maintenance ex vivo, and we established an AFT stromal line RalB knockdown (KD), *RalB* being a gene recently shown to impair EV release in mammalian cells (Hyenne et al., 2015). We first validated the decrease in RalB expression (Fig. 3 E) and EV release (Fig. 3, F and G) in comparison with control (shSCR). Then, RalB KD (shRalB) and control (shSCR) AFT cells were cocultured for 96 h with LSK cells and flow cytometry analysis, and clonogenic assays showed that RalB KD AFT cells less efficiently supported LSK cells as indicated by the significant ($P < 0.05$) decrease in the percentage of CD45$^+$ cells (Fig. 3, H and I) and in the number of clonogenic progenitors after coculture (Fig. 3 J). Finally, LSK cells were cultured with AFT conditioned medium (CM) depleted from EVs (−110,000 *g*) or not (−300 *g*) by ultracentrifugation steps. Only LSK cells cultured in CM depleted of EV completely lost their clonogenic potential after 96 h (Fig. 3 K). Collectively, these data indicate that AFT EVs are functionally effective in immature hematopoietic cells and contribute to the ability of AFT cells to maintain LSK cells ex vivo.

AFT and BFC EVs have distinct RNA signatures

We used high-throughput sequencing to compare the molecular signatures of AFT and BFC EVs to those of their cells of origin. Small RNAs and mRNAs were isolated, and the libraries were sequenced using next-generation sequencing Illumina technology. Reads were aligned on the reference genomes using the *Bowtie* and *Tophat* tools available on the Galaxy server (Fig. 4 A).

Global analyses of the small RNA libraries revealed three major differences between EVs and cells. First, cell libraries included ∼80% of miRNAs, in sharp contrast with EV libraries that exhibited only ∼10% of miRNAs (Figs. 4 B and S3 A). Second, small RNA libraries from both AFT and BFC EVs displayed a significant amount of ribosomal RNAs (69 and 60%, respectively) when compared with cells (Fig. 4 B). Third, EV libraries were enriched in tRNA (6 and 7% in AFT and BFC EVs, respectively) when compared with cells (1.7 and 1.6% in AFT and BFC, respectively). Analyzing the poly-A RNA libraries, we looked for the gene types of the most abundantly expressed genes (reads per kilobase per million mapped reads [RPKM] > 100) in each library. EVs had less protein-coding RNAs than the cells

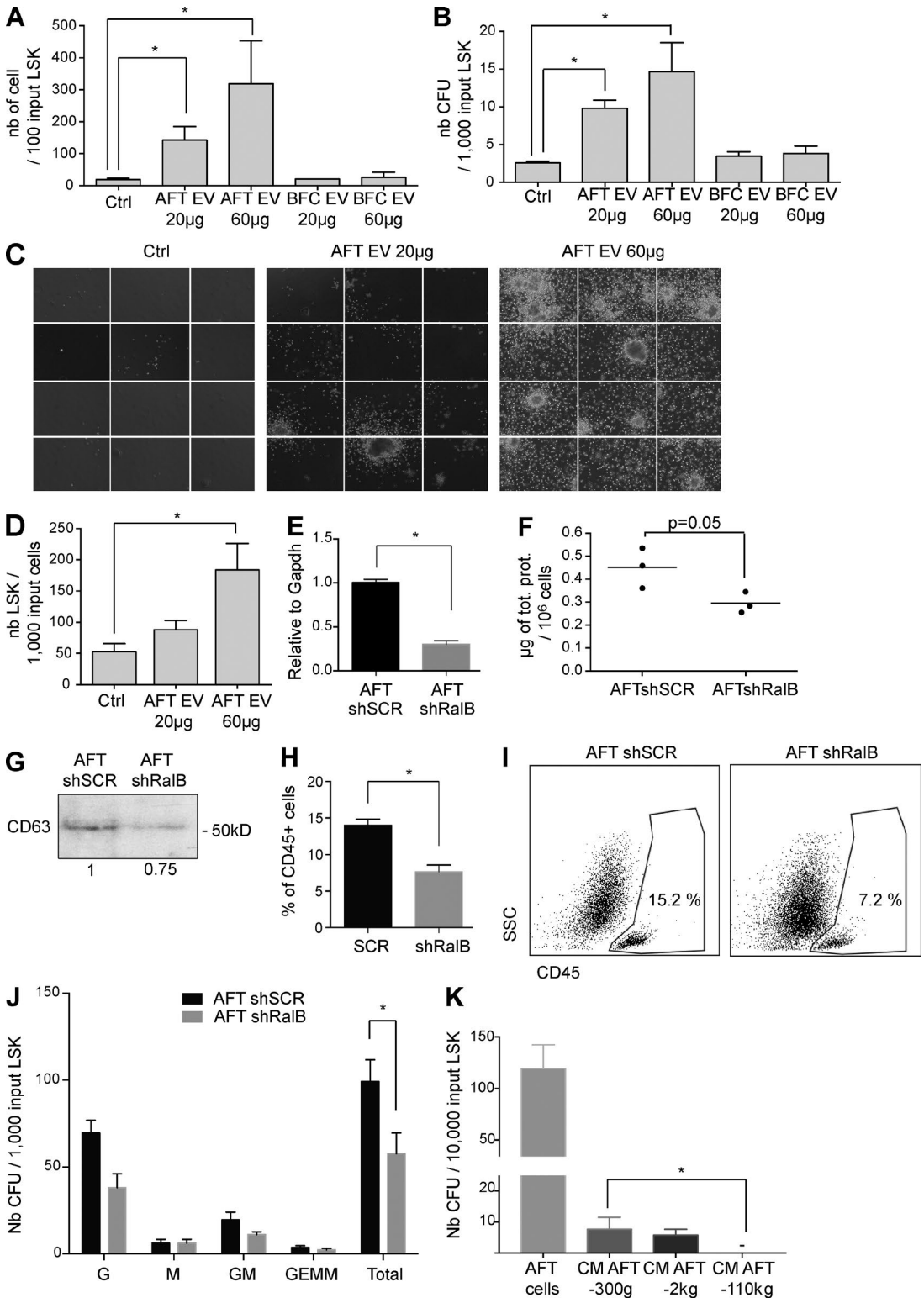

Figure 3. **Role of stromal EVs in HSPC maintenance ex vivo.** (A) Proliferation of LSK cells cocultured 96 h with two quantities of stromal EVs in the absence of cytokines (n = 6). (B) Clonogenic potential of LSK cells cocultured 96 h with two quantities of stromal EVs (n = 6). (C) Representative micrographs depicting colony-forming units (CFUs). Note the difference in number (nb) and size between the two doses of AFT EVs. These figures are composites of multiple separate images. (D) Dose effect of AFT EVs on the maintenance of LSK cells after 96 h (n = 3). (E) Quantitative PCR measurement of RalB expression in AFT-*shSCR*– or AFT-*shRalB*–transduced cells. (F) Total protein quantification of EVs collected after culture of AFT-*shSCR* or AFT-*shRalB* cells. (G) Western blot analysis of CD63 protein expression in AFT-*shSCR* or AFT-*shRalB* cells. (H) Percentage of CD45$^+$ cells after LSK/AFT-*shSCR* or AFT-*shRalB* cocultures during 96 h. (I) Representative flow cytometry analysis of CD45 expression in cocultures. (J) Clonogenic potential of LSK cocultures with AFT-*shSCR* or AFT-*shRalB* cells (n = 3). G, granulocyte; GEMM, granulocyte/erythrocyte/macrophage/megakaryocyte; GM, granulocyte/macrophage; M, macrophage. (K) Clonogenic potential of LSK cocultures with AFT cells or different fractions of AFT CM after sequential centrifugation at 300 *g* (CM AFT-300g), 2,000 *g* (CM AFT-2kg), and 110,000 *g* (CM AFT-110kg; n = 3). Error bars show SEM. *, $P < 0.05$.

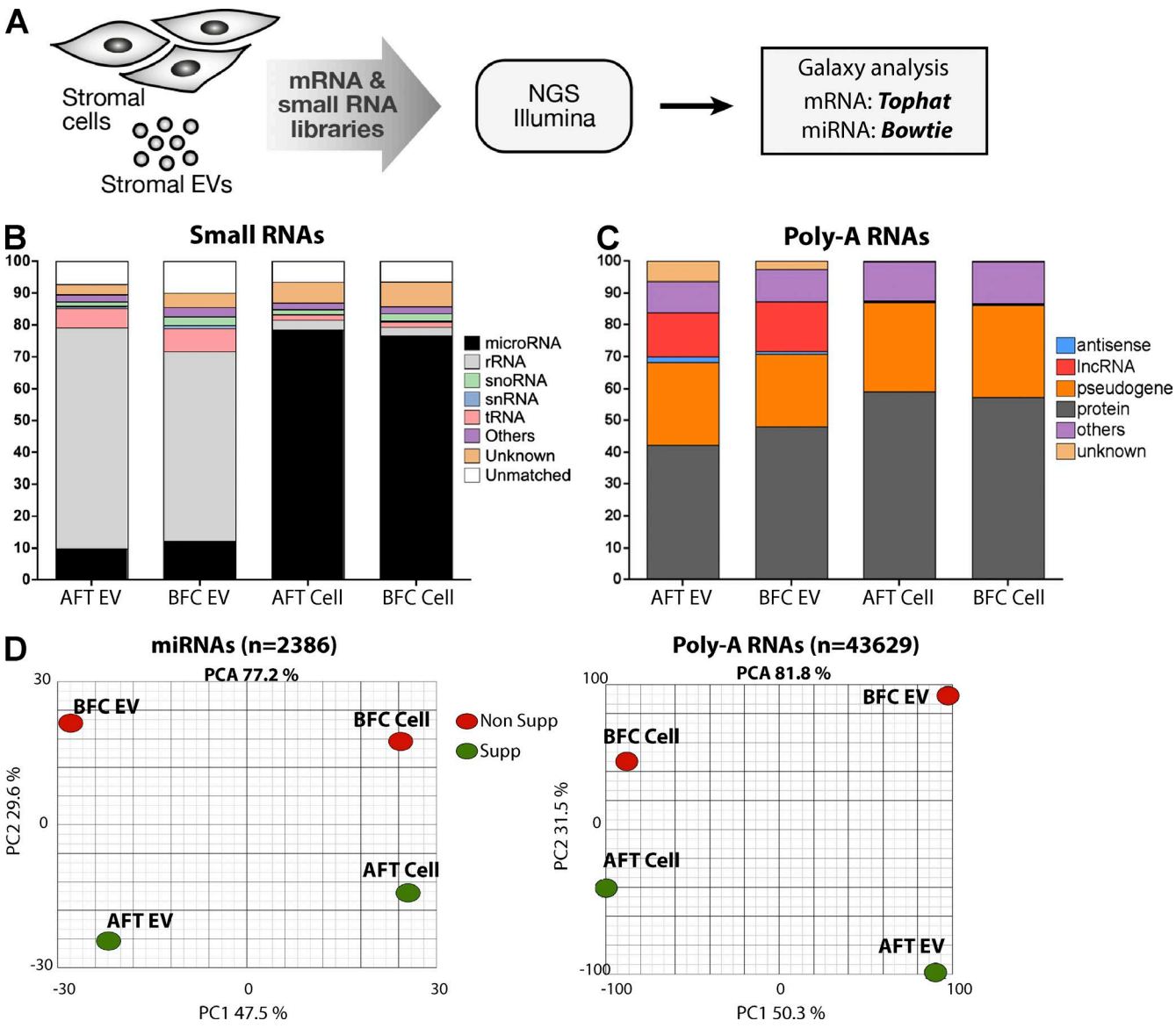

Figure 4. **RNA-seq analysis of the molecular signatures displayed by the stromal cells and the EV.** (A) Workflow chart of the RNA-seq analysis. NGS, next-generation sequencing. (B and C) Global analysis of the small RNA (B) and poly-A–RNA (C) libraries. For the small RNA libraries, all the sequenced reads are represented, and for the poly-A–RNA libraries, only the most abundant genes (RPKM > 100) are represented. (D) PCA of the global miRNA (left) and poly-A RNA (right) transcriptomes.

of origin (Fig. 4 C) but were enriched in antisense and lncRNAs (e.g., for AFT, six- and 68-fold change, respectively). Moreover, in AFT, 6.21% of the transcripts identified in EVs were not characterized, contrasting with cells for which unknown transcripts constituted only 0.14% of the total (Fig. 4 C).

To globally determine whether a specific molecular signature could discriminate EVs from cells and discriminate EVs from cells with differing HSPC-supportive capacities, we performed principal component analyses (PCAs) of the entire sets of miRNAs (Fig. 4 D, left) and poly-A RNAs (Fig. 4 D, right). With respect to miRNAs, this unsupervised analysis allowed discriminating EVs from cells regardless of the cell type of origin according to the first component PC1 as well as HSPC-supportive or -nonsupportive capacity regardless of the cell compartment (EVs or whole cells), according to the second component PC2. Similar results were found when poly-A RNAs were considered. These data indicate that the EV signatures are strikingly different from that of the cell counterparts and that the RNA cargo of AFT EVs is clearly distinct from that of BFC EVs.

AFT EVs carry specific mRNA and miRNA signatures

We then used pairwise comparisons to identify the specific molecular signature of AFT EVs. To this aim, we made pairwise comparisons of the gene expression profiles (miRNAs and poly-A RNAs) of EVs (AFT EV vs. BFC EV) and cells (AFT CELL vs. BFC CELL) and EVs versus cells for each of the lines (AFT EV vs. AFT CELL and BFC EV vs. BFC CELL). Data were filtered with p-values <0.0001 and fold changes ≥2 or ≤−2 (Fig. S3 B). As previously described (Charbord et al., 2014), AFT and BFC cells exhibited specific and contrasted mRNA and miRNA signatures; this was also the case for their related EVs (Fig. S3). Furthermore, the EV-specific and

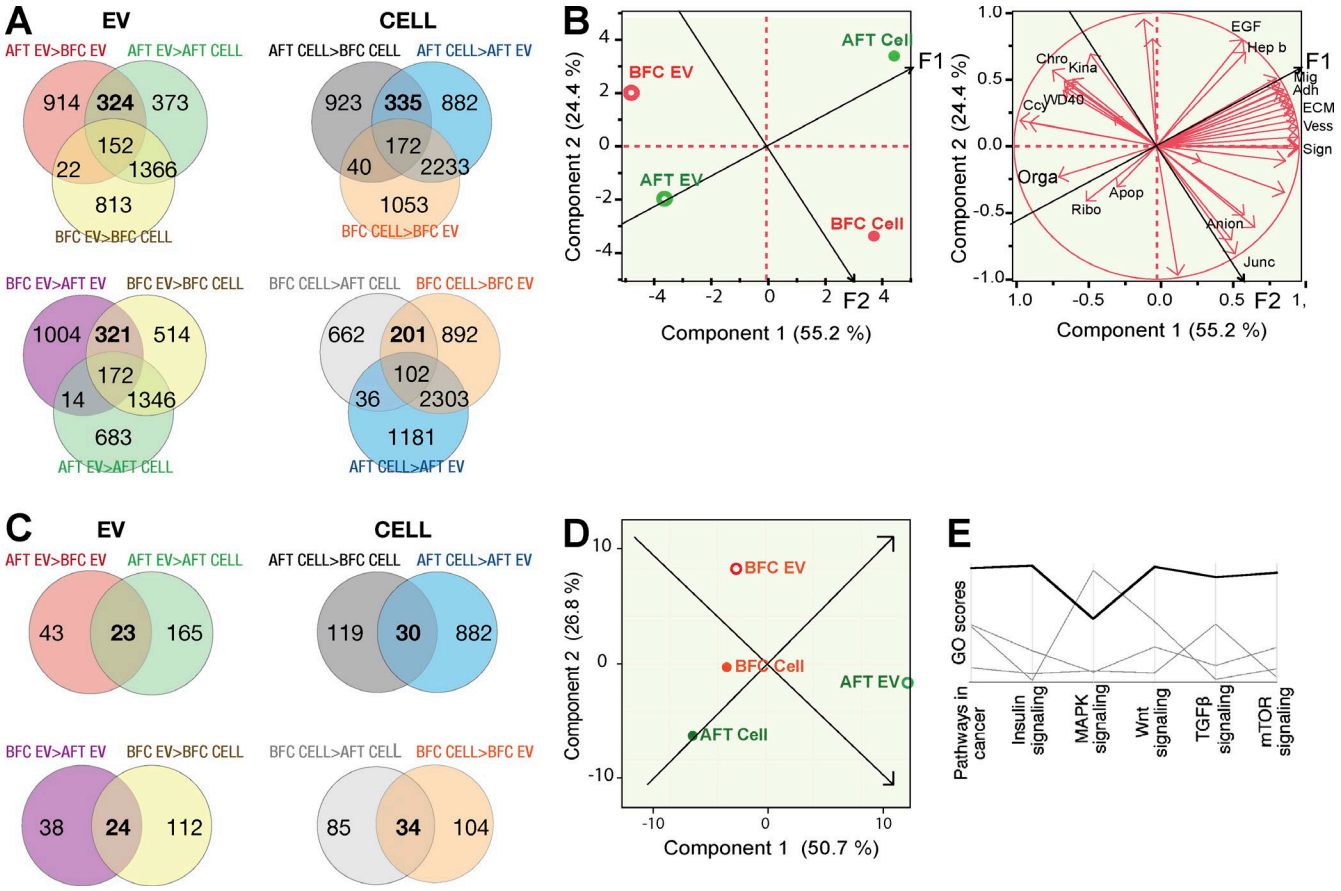

Figure 5. **Analysis of the poly-A RNA and small RNA signatures.** (A) Venn diagrams showing the intersections of the specific mRNA sets. DEGs between categories are filtered (P < 0.0001 and fold change >2); intersections and subtractions are performed to obtain minimal gene sets specific for each category. Numbers in bold represent the gene set specific for each category and were used to perform GO analysis using the DAVID database. (B) PCA based on the GO scores obtained for each gene set (left). The loading plot (right) shows the most relevant categories correlated with the axes. Adh, cell adhesion; Anion, anion channel activity; Apop, apoptosis; Ccy, cell cycle; Chro, chromosome; EGF, EGF motif; Hep b, heparin binding; Junc, cell junction; Kina, kinase; Mig, migration; Orga, nonmembrane-bound organelle; Ribo, ribosome; Sign, signal; Vess, vessel; WD40, WD40 repeat. (C) Venn diagrams showing the intersections of the specific miRNA sets. Differentially expressed miRNAs between categories were filtered (P < 0.0001 and fold change >2), and intersections were performed to obtain minimal miRNA sets specific for each category. Numbers in bold represent the gene set specific for each category and were used to perform GO analysis of the miRNA-predicted targets using the miRsystem database. (D) PCA based on the GO scores obtained for each gene set. (E) Enrichment scores of GO categories of the putative targets of each specific miRNA set (*miRsystem*).

cell-specific gene sets were strikingly different, which indicates that RNAs are specifically filtered in their transit toward the extracellular compartment (Fig. S3).

To identify the transcripts specifically expressed in AFT EVs (AFT EV gene set), we selected the mRNAs significantly expressed (P < 0.0001) at higher levels (fold change >2) in AFT compared with BFC EVs (AFT EV > BFC EV) and with AFT cells (AFT EV > AFT CELL) and identified the intersecting gene set, and then we subtracted from this gene set the mRNAs that were significantly expressed at higher levels in BFC EVs in comparison with BFC cells (BFC EV > BFC CELL). We proceeded likewise for the transcripts specific for AFT cells, BFC EVs, and BFC cells (Fig. 5 A). We found 324 mRNAs specifically enriched in AFT EVs, 321 mRNAs in BFC EVs, and 335 and 201 in AFT and BFC cells, respectively (Fig. 5 A).

Using the Database for Annotation, Visualization, and Integrated Discovery (DAVID), we identified the gene ontology (GO) categories corresponding with each gene set. 34 categories with significant enrichment scores (nominal P < 0.05) were found. PCAwith the four GO sets (AFT EV, AFT CELL, BFC EV, and BFC CELL) and the 34 categories revealed that PC1 corresponded with the factor cell structure ("cell" on the right and "EV" on the left of the score plot). Moreover, rotation conserving orthogonality of the components by 34° was allowed to disclose two new axes (F1 and F2) corresponding with minimal projections of the AFT (AFT EV and AFT CELL) and BFC (BFC EV and BFC CELL) gene sets. On the loading plot, many of the supportive canonical categories described previously (e.g., "ECM," "cell adhesion," "EGF-like motif," and "heparin binding"; Charbord et al., 2014) were positively correlated to F1, whereas the "anion channel activity" and "cell junction" categories were characteristic of BFC cells (correlated to F2). "Ribosome," "nonmembrane-bound organelle," and "apoptosis" characterized AFT EV (negatively correlated to F1), whereas "chromosome," "cell cycle," "kinase," and "WD40 repeat" characterized BFC EV (negatively correlated to F2; Fig. 5 B). Ingenuity pathway analysis (IPA) was also performed, and among the top predicted networks for AFT EVs were "protein synthesis," "hematological system development and function," and "endocrine system disorders, immunological disease" (Fig. S4 A). Using IPA, the main cellular function associated with the AFT EV RNAs was "cell death and survival,"

with decreases of "apoptosis" (P = 2.06E−03; z score −2.4) and "cell death" (P = 2.29E−02; z score −2.2) functions. Among the 324 mRNAs specifically enriched in AFT EVs, 32 were associated with a decrease of apoptosis, and some of them, such as *Fth1*, *Peg10*, *Taf10*, *Mt1*, and *Bag1*, were highly enriched (2,337, 2,058, 181, 130, and 106 RPKM, respectively; Table S1). Other mRNAs that belong to the category "protein synthesis" and transcripts coding for "ribosomal proteins," such as *Rps27*, *Rpl23*, and *Rpl38*, were among the most abundant. Collectively, these data indicate that the gene set specific for AFT EVs corresponds with well-defined biological processes such as the regulation of apoptosis and is clearly distinct from those of AFT cells and BFC EVs.

A similar approach was performed for the miRNA datasets. We selected the miRNAs significantly expressed (P < 0.0001) at a higher level (fold change >2) in AFT EVs compared with BFC EVs (AFT EV > BFC EV) and to AFT cells (AFT EV > AFT CELL), and we identified the intersecting gene set without any subtraction. We found 23 miRNAs specifically enriched in AFT EVs and 24, 30, and 34 miRNAs specifically enriched in BFC EVs, AFT cells, and BFC cells, respectively (Fig. 5 C). Using the miRsystem, we identified the putative targets of each miRNA set and its associated GO pathways. There were 161 KEGG (Kyoto Encyclopedia of Genes and Genomes) pathways with associated enrichment scores that were used to perform PCA on the four datasets. Although PCA did not discriminate samples along clear biological categories, PC1 clearly segregated the AFT EV samples (Fig. 5 D). Several pathways involved in hematopoiesis and/or cell survival, such as insulin, mTOR, and TGFβ pathways, were specific targets of the AFT EV–specific miRNAs (Fig. 5 E). Furthermore, among the 23 miRNAs specific for AFT EVs, some of them, such as miR-221, miR-451, miR-142, miR-144, and miR-223, were not only highly represented in AFT EVs but were also strongly enriched in EVs when compared with cells ($\log_2$FC = 2.08 – 11.42), suggesting specific EV-addressing mechanisms (Table S1). Interestingly, these five most abundant miRNAs putatively targeted 26, 17, and 21 genes belonging to the aforementioned pathways.

AFT EVs transfer mRNAs and miRNAs in LSK cells and inhibit apoptosis

We studied the transfer of two RNAs from AFT EVs to LSK target cells. We focused on two genes, *Peg10* (paternally expressed gene 10) and *Bag1* (BAG family molecular chaperone regulator 1), highly enriched in and specific to AFT EVs (Table S1) and involved in the negative regulation of apoptosis (Götz et al., 2005; Peng et al., 2015). 6 h after contact with AFT EVs, the mRNA levels of *Peg10* and *Bag1* in LSK cells were increased eight- and 1.6-fold, respectively (Fig. 6 A). A similar approach on miRNAs showed that miR-451a-5p and miR-221-3p were more abundant in LSK cells after contact with AFT EVs (1.5- and 2-fold change, respectively; Fig. 6 A). We then analyzed the impact of AFT EVs on HSPC apoptosis. LSK cells were cocultured with or without AFT EVs in the absence of cytokines for 18 h. Whereas 8.6% of LSK cells were preapoptotic (annexin V^+/$7AAD^-$) when cultured without cytokines, only 4.4% displayed an identical status when AFT EVs were added (Fig. 6 B). These results suggest that the short-term exposure of LSK cells to AFT EVs protected them from apoptosis. We then tested whether Peg10 and miR-451 misexpression may affect apoptosis of lineage-negative (Lin^{neg}) hematopoietic progenitors that responded similarly to AFT EV treatment as LSK cells (Fig. S4, B–D). We used siPeg10 and mimic–miR-451 to inhibit or increase the expression of the corresponding genes, respectively (Fig. 6, C and E). Down-regulation of Peg10 slightly increased apoptosis in Lin^{neg} cells (Fig. 6 D). Conversely, miR-451 overexpression had weak to no effect on Lin^{neg} cell apoptosis (Fig. 6 F). Similar but weaker effects were found on LSK cells (Fig. S4 E). Collectively, these results suggest a multifactorial antiapoptotic effect of AFT EVs on HSPCs likely mediated by multiple regulators.

Modification of the HSPC gene profile after coculture with AFT EVs

We finally studied the global modification of the LSK transcriptome induced after AFT EV exposure. RNA was extracted from naive LSK cells directly after cell sorting (LSK t0) and directly after 18 h of culture with (LSK + EV 18 h) or without AFT EVs (LSK 18 h). Gene expression microarray analysis (n = five per setting) was performed on these three conditions. PCA performed on the entire transcriptome gene set showed a clear segregation between LSK t0 and cultured LSK cells regardless of EVs, the first two components accounting for 32.3% of the variance (Fig. 7 A). This unsupervised analysis thus revealed that major gene expression modifications were induced by the ex vivo culture of LSK cells. To highlight the differentially expressed genes (DEGs) between LSK cells cultured with or without AFT EVs, one-way ANOVA was performed, and data were filtered with P < 0.05 for statistical significance between gene expression levels. Based on this statistical analysis, 2,051 DEGs were identified. PCA using members of this gene set as variables and the 15 samples as observations revealed a clear segregation between the different LSK cell populations (Fig. 7 B), the first two components accounting for 52.3% of the variance. Hierarchical clustering using Euclidean distance highlighted five main gene clusters (Fig. 7 C). Cluster I included genes that were down-regulated in naive LSK cells and became up-regulated in LSK cells cultured for 18 h but remained down-regulated when LSK cells were cultured for an identical time in the presence of AFT EVs. Clusters II and III included genes up-regulated in naive LSK cells and LSK cells cultured for 18 h in the absence of EVs, respectively. Cluster IV included genes up-regulated in naive LSK cells and stayed up-regulated when LSK cells were cultured in the presence of AFT EVs. Lastly, cluster V included genes up-regulated specifically in LSK cells cultured in the presence of AFT EVs (Fig. 7 C). GO enrichment analyses were performed on the five clusters (Fig. 7 D). Of particular interest, cluster IV was enriched in genes involved in protein translation or belonging to chemokine pathways. The category "protein translation," found enriched in AFT EVs (Fig. 5 A), was also highly enriched in naive LSK cells (cluster II; Fig. 7 D). In cluster V, the categories "extracellular region," "signal," and "secreted" were among the most enriched, in agreement with similar enrichment in cells of supportive versus nonsupportive lines (Charbord et al., 2014). Of note, highly expressed genes in AFT EVs (RPKM >50) were significantly (P < 4.3E−16) up-regulated in LSK cells after contact with AFT EVs, whereas genes absent (RPKM = 0) in AFT EVs did not statistically vary in LSK cells after contact with EVs (Fig. 7 E). Moreover, we found that 54% (n = 28) of the genes most highly up-regulated in LSK cells after culture with EVs (fold change >2) were strongly enriched in AFT EVs (Fig. 7 F). Among them, Peg10 was one of the most up-regulated after contact with EVs (Fig. 7 G). Concerning the genes down-regulated in

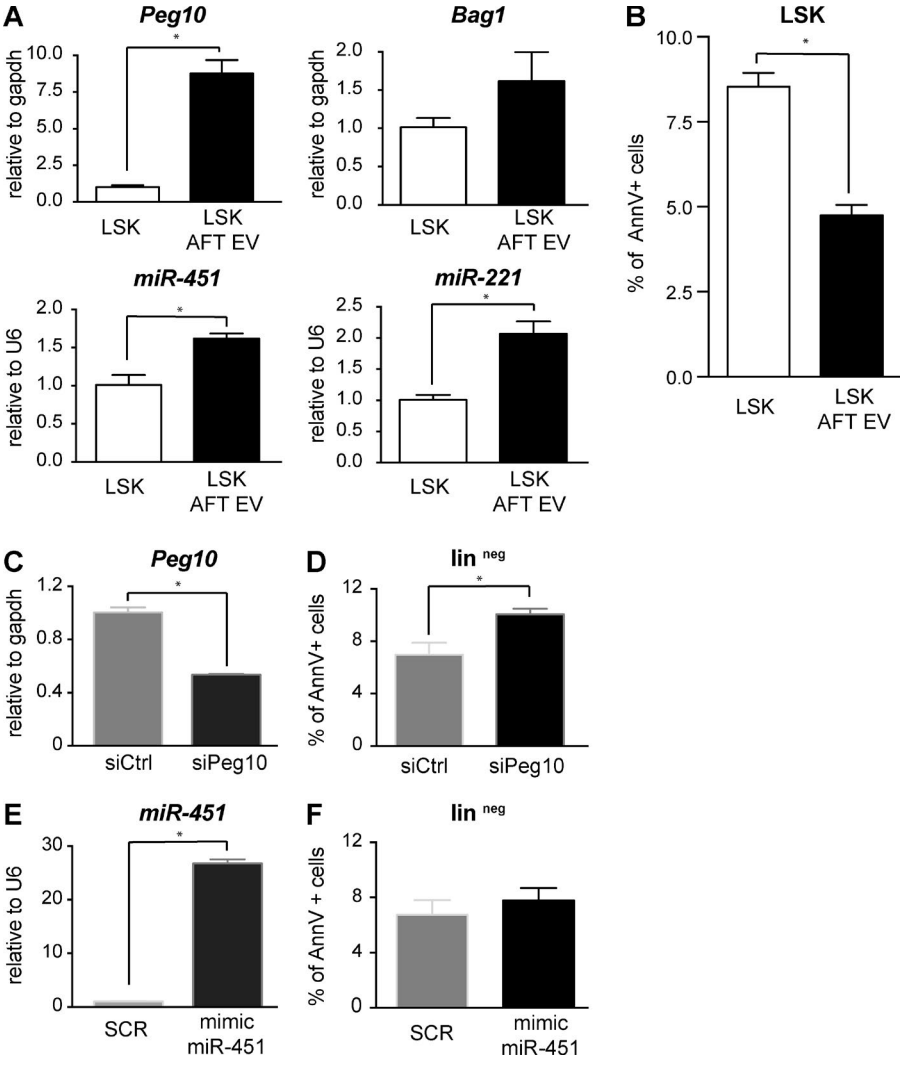

Figure 6. **mRNAs and miRNAs transfer from AFT EVs to LSK cells and apoptotic assay.** (A) Expression changes of *Peg10* and *Bag1* mRNAs and *miR-451* and *miR-221* miRNAs in LSK cells after contact with AFT EVs. Quantitative PCR analyses were normalized using GAPDH for mRNAs and U6 internal control for miRNAs ($n = 3$). (B) Measurement of apoptosis by annexin V (AnnV) and 7AAD staining in LSK cells cocultured for 18 h with or without AFT EVs in the absence of cytokines ($n = 3$). (C and E) Expression of *Peg10* and *miR-451* in lineage-negative cells transfected with siPeg10 (C) or mimic-451 (E). (D and F) Measurement of apoptosis using annexin V and 7AAD staining in lineage-negative cells transfected with siPeg10 (D) and mimic-451 (F; $n = 3$). All the cultures were performed in absence of cytokines. Error bars show SEM. *, $P < 0.05$.

LSK cells after culture with EVs, 9% ($n = 33$) were predicted or validated targets of the four most abundant miRNAs in AFT EVs (Fig. S4, B and C). Collectively, these data suggest that EV cargo could be directly transferred into LSK cells and subsequently modulate the gene expression profile associated with their maintenance ex vivo.

Discussion

By taking advantage of two stromal lines with widely differing capacities to support HSPCs ex vivo, we provide evidence that EVs are released by stromal cells and taken up by HSPCs and play a critical role on HSPCs. Specifically, we show that EVs produced by the supportive AFT stromal lines are actively taken up by HSPCs both ex vivo and in vivo and support their survival and clonogenic potentials in culture. One of the most notable findings of our study is the selective uptake by HSPCs of EVs produced by the supportive stromal line but not those released by the nonsupportive one. EV uptake relies on the expression of transmembrane proteins such as tetraspanins and integrins and also on the combinations of ligands and receptors at the surface membrane of the secreted vesicles and target cells (Mulcahy et al., 2014). We observed that AFT EVs express higher amounts of the tetraspanin CD9 than BFC EVs. Because CD9 has been demonstrated to be essential for EV uptake by dendritic cells (Morelli et al., 2004) and to physically interact with the cytokine receptor c-kit expressed by HSPCs (Anzai et al., 2002), a role for CD9 in our system may be hypothesized. Further EV marker characterization and high-throughput analysis of the proteins expressed at the surface membrane of EV will be necessary for understanding the precise mechanisms involved in the specific uptake of stromal EVs by HSPCs.

To decipher how stromal EVs mediate their effects on HSPCs, we explored in detail the molecular signature of EVs released by the stromal lines AFT and BFC and of HSPCs before and after culture with AFT EV. Regardless of the cells of origin (supportive or nonsupportive), we found that EVs were enriched in lncRNAs. Interestingly, a recent study showed that lncRNAs are involved in the control of HSPC function (Luo et al., 2015), emphasizing the putative role of the lncRNAs carried by AFT EVs, which should be further investigated. AFT EVs are enriched in transcripts coding for genes implicated in protein synthesis and the regulation of apoptosis. Enrichment in genes implicated in protein synthesis has already been shown in EVs released by mast cells and taken up by human $CD34^+$ blood cell progenitors (Ekström et al., 2012). The enrichment of genes implicated in the regulation of apoptosis is consistent with the result of our biological assays showing a decrease of annexin V^+ LSK cells exposed to AFT EVs. Several mRNAs

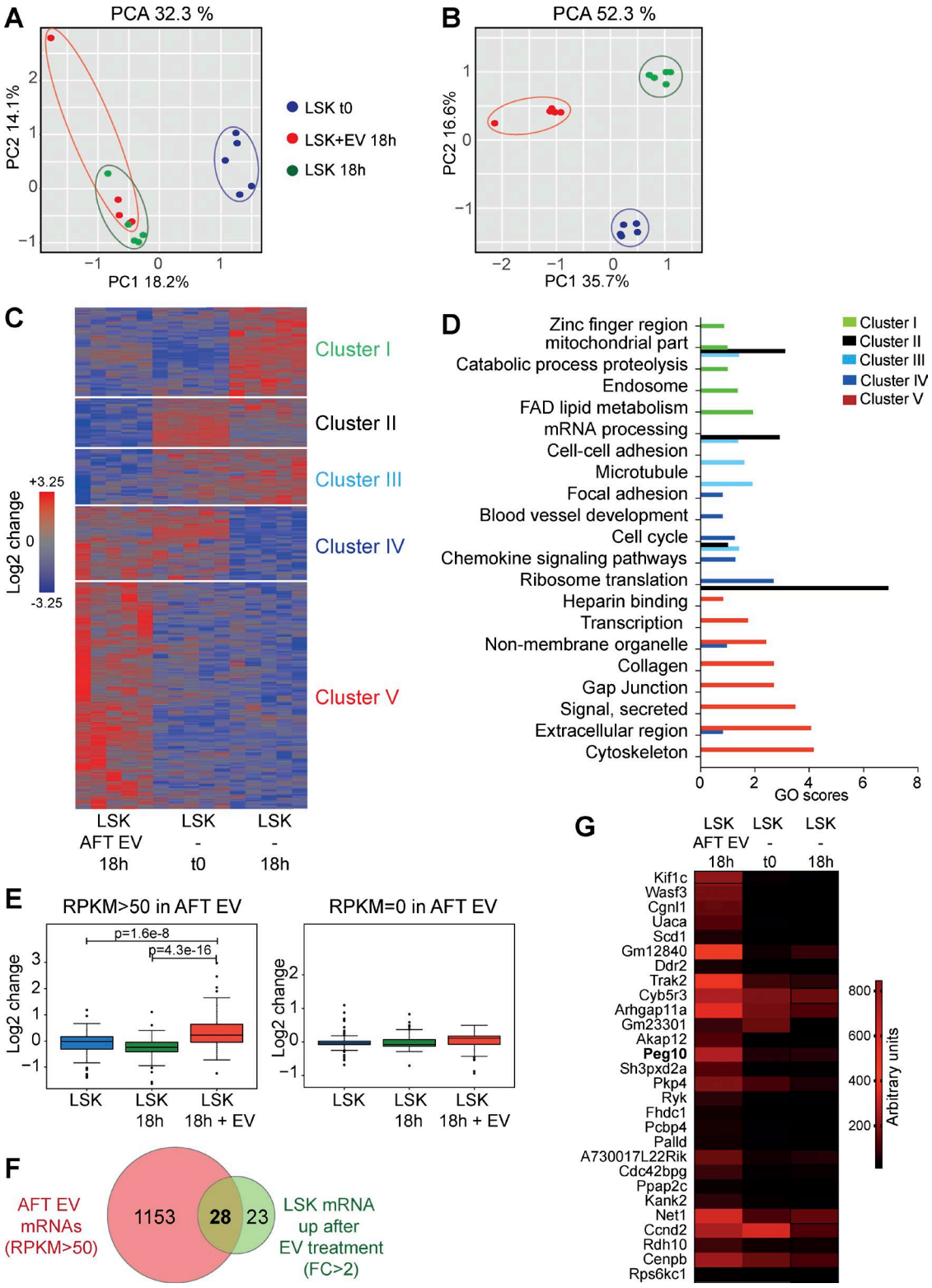

Figure 7. **RNA signature changes in LSK cells after contact with AFT EVs.** (A) PCA on the global transcriptomes of LSK-naive cells (LSK t0) and LSK cells cultured without cytokines during 18 h with or without AFT EVs (LSK+EV 18h and LSK 18h, respectively). (B) PCA based on the 2,051 DEGs between LSK 18 h and LSK 18 h + EV (one way ANOVA; $P < 0.05$). (C) Heat map and *k*-mean hierarchical clustering based on the 2,051 DEGs revealed five gene clusters. (D) GO enrichment analysis of the clusters. FAD, flavin adenine dinucleotide. (E) Relative mean expression of highly expressed AFT EV genes (RPKM >50) in LSK cells before and after contact. (F) Venn diagram of the most abundant genes in AFT EVs and genes highly up-regulated in LSK cells after EV treatment. FC, fold change. (G) Heat map of the common genes in F.

known to negatively regulate apoptosis, including *Peg10* and *Bag1*, are strongly enriched in AFT EVs, and their expression increases in LSK cells after culture with AFT EVs. *Peg10* enrichment is of interest because this molecule has been shown to protect cells from apoptosis by stabilizing caspase-3 and -8, and its impaired expression in HSPCs has resulted in apoptosis (Peng et al., 2015). These results are also in agreement with the reported role of EVs derived from MSCs in the survival of hematopoietic progenitors (De Luca et al., 2016; Wen et al., 2016) and in the protection against apoptosis in a renal injury setting (Zhou et al., 2013).

Regarding the miRNA signature, we also found different EV-to-cell contrasts for AFT versus BFC lines. MiRNA-221, miRNA-451, and miRNA-142, for example, are highly enriched in AFT EVs. Because these miRNAs have been reported to be specifically enriched in EVs derived from MSCs (Collino et al., 2010), they may be components of an MSC-specific miRNA signature. Moreover, miRNA-451 has been involved in the regulation of stemness of the side population in multiple myeloma via the PI3K–AKT–mTOR signaling pathway, conferring, among others, apoptosis resistance (Du et al., 2015), and miRNA-221 has been predicted to influence endothelial cell apoptosis (Qin et al., 2015).

Importantly, we show that the gene expression profile of LSK cells is profoundly influenced by AFT EVs. Our data suggest that the EV RNA cargo is directly delivered into LSK cells, with subsequent modifications of gene expression. Among the biological processes enriched in LSK cells exposed to AFT EVs, we find the categories "secreted" and "signal." We and others have reported that these pathways are strongly representative of the HSPC-supporting capacity of stromal cells (Charbord et al., 2014; Lim et al., 2016). For example, we find that the secreted chemokine Cxcl12, the cytokine Ptn, and the ECM component Col4A3 are up-regulated in LSK cells after culture with AFT EVs, suggesting that stromal EVs maintain HSPCs through the direct transfer of HSPC niche factors.

In conclusion, our results indicate that EVs delivered by stromal cells and taken up by HSPCs modulate HSPC gene expression and functional behavior, complementing the classical view whereby intercellular communication is effective through direct ligand-to-receptor interaction (cell-to-cell or cell-to-ECM contact). Our work calls for further preclinical studies with interesting applications in regenerative medicine, including cell therapy protocols for delivering specific molecules to HSPCs to efficiently support their maintenance and/or amplification in stromal-free conditions.

Materials and methods

Stromal cell cultures and EV extraction

FL stromal lines (AFT024 and BFC012) were generated from E14.5 embryos (Moore et al., 1997). Stromal cells were cultured on 0.1% gelatin-coated flasks in high-glucose DMEM supplemented by 10% FCS, 1% glutamine and penicillin-streptomycin, and 55 µM β-mercaptoethanol, and maintained at 33°C and 5% CO_2 in a humid atmosphere.

EVs were isolated from supernatants of 9×10^7 stromal cells cultured 96 h in advance in EV-free FCS medium according to previously described protocol (Théry et al., 2006). 30 min before supernatant collection, calcium ionophore was added to the medium (1 µM) to increase EV release (Savina et al., 2003). Two steps of centrifugation were performed (300 *g* for 5 min and 2,000 *g* for 20 min), and then cell- and debris-free supernatants were filtered through a 0.2-µm filter, ultracentrifuged at 110,000 *g* for 2 h at 4°C (SW32 rotor; Beckman Coulter), washed in PBS, and submitted to a second ultracentrifugation.

HSPC extraction

BM was obtained from adult C57BL/6 female mice (3–10 mo of age). Mice were bred at Janvier Labs and maintained in the animal facility of the Laboratory of Developmental Biology at University Pierre and Marie Curie (UMR7622; Centre National de la Recherche Scientifique) according to institutional guidelines. BM lineage-negative cells were first isolated by depletion of hematopoietic lineage markers expressing cells using MACS columns (Miltenyi Biotec). Cells were then stained with phycoerythrin (PE)-conjugated anti–Sca-1 and allophycocyanin (APC)-conjugated anti–c-kit antibodies and purified with an Influx 500 cell sorter (BD).

Cell transfection

AFT-shSCR and -shRalB cells were obtained after infection by pLKOshSCR or pLKOshRalB lentivirus (provided by V. Hyenne, Institut National de la Santé et de la Recherche Médicale, Paris, France, and produced in 293T cells), and puromycin selection was done as previously described (Hyenne et al., 2015). AFT-CD63-GFP cells were sorted by flow cytometry after transfection with hCD63-EGFP vector (a gift from C. Théry, Institute Curie, Paris, France).

Hematopoietic lineage-negative cells and LSK cells were transfected with siRNA and mimicRNA at 60 nM (Ambion) using DOTAP according to the manufacturer's protocol (Sigma-Aldrich).

Electron microscopy

AFT and BFC stromal cells were plated in six-well plates. Once they reached 70% confluence, they were fixed with 4% paraformaldehyde and 1% glutaraldehyde in 0.1 M sodium cacodylate buffer, pH 7.2, for 3 h at room temperature, washed with cacodylate buffer, postfixed in 1% osmium tetroxide, progressively dehydrated in a graded ethanol series (50–100%), and embedded in epon. Ultrathin (70–80 nm) sections were cut from the polymer with a microtome, placed on copper grids, and briefly stained with uranyl acetate and lead citrate.

The EV pellets were pooled in 100 µl of PBS after ultracentrifugation of the CM. Then, 10 µl of the samples were applied on a 300 mesh EM grid with lacey carbon. Excess sample was removed by blotting once for 1–2 s with filter paper. The blotted grids were plunged into liquid ethane that was kept in equilibrium with solid ethane. After vitrification, the grid was stored under liquid nitrogen until further use.

Flow cytometry analyses of EVs

EV pellets were resuspended in 0.2-µm filtered PBS (volume 1/2,000 of CM used for extraction). EVs were then stained with PE anti-CD9 (124805) and APC anti-CD63 mouse antibodies (143905; BioLegend) or with corresponding isotype controls. After 1 h incubation in the dark at 4°C under agitation, PBS was added, and each sample was analyzed by an Influx flow cytometer (MACSQuant; BD) using a novel high-resolution flow cytometry–based method recently developed for quantitative high-throughput analysis of individual immunolabeled nano-sized vesicles (van der Vlist et al., 2012).

Western blot

EV pellets were resuspended in 50 µl of lysis buffer (0.15 M NaCl, 5 mM EDTA, pH 8, 1% Triton X-100, and 10 mM Tris-HCl, pH 7.4), and protein contents were quantified using a BCA protein assay kit according to the manufacturer's protocol (Thermo Fisher Scientific). Protein extracts from EV pellets and cell lysates were prepared with Laemmli buffer in nonreductive conditions, heated at 95°C for 5 min,

and separated on 15% polyacrylamide gels before transfer to a nitrocellulose membrane (Hybond ECL plus; Thermo Fisher Scientific). Membranes were blocked in 5% nonfat milk and incubated with the anti-CD9 (H-110; Santa Cruz Biotechnology, Inc.), -CD63 (H-193; Santa Cruz Biotechnology, Inc.), -TSG101 (C-2; Santa Cruz Biotechnology, Inc.), LAMP1 (1D4B; Abcam), and α-tubulin antibodies (4074; Abcam) followed by the horseradish peroxidase–coupled secondary antibody and then were subjected to enhanced chemiluminescence.

RNA extraction

EV pellets and their cells of origin were suspended in TRIzol (Invitrogen), and RNA extraction was performed according to the manufacturer's protocol. RNA amounts and integrity were quantified on a nanodrop spectrophotometer and analyzed using an Agilent 2100 Bioanalyzer (Agilent Technologies).

EV uptake

EV pellets were labeled with the green fluorescent dye PKH67 (Sigma-Aldrich) according to the manufacturer's protocol. The staining reaction was stopped by adding EV-free medium, and PKH67-stained EVs were washed three times with PBS by ultracentrifugation (110,000 *g* for 2 h at 4°C) to remove excess dye. The EV pellets were suspended in Myelocult TM 5300 (STEMCELL Technologies). For LSK uptake, 30,000 BM LSK cells were plated for each tested condition, and stained EVs were added to the culture medium supplemented with hydrocortisone (1 µM), stem cell factor (SCF), thrombopoietin, and Flt3-L (5 ng/ml) to maintain live LSK cells. Acquisition was performed after 24 h using an ImageStreamX Imaging Flow Cytometer (Amnis). A 60× magnification was used for all samples. PKH67 was excited with 100 mW of 488-nm argon laser, and fluorescence was collected at 505–560 nm. Data analyses were performed using the IDEAS software (Amnis). For total BM uptake, the EV suspensions were added to 10^6 BM cells in DMEM supplemented with 10% FCS, SCF, IL-6, IL-3, and Flt3-L at 10 ng/ml, and cells were analyzed by flow cytometry 24 h later. For in vivo uptake, intrafemoral injections of EVs (100 µg) were performed, and BM was recovered 24 h later for flow cytometer analysis. BM cells were stained with anti-CD45 (BlueViolet510), anti-lineage markers (APC), anti-CD117 (PEC7), and anti–Sca-1 (PE) antibodies (BioLegend), and the acquisition was performed on a MACSQuant flow cytometer.

Cocultures of 15,000 AFT-CD63-GFP cells and 15,000 LSK cells were performed during 96 h until cells were harvested, stained with anti-CD45 (PE), and analyzed with ImageStreamX as described in the previous paragraph.

Hematopoietic assays

LSK cells were cocultured for 96 h at 37°C and 5% CO_2 in long-term medium (Myelocult; M5300; STEMCELL Technologies) with stromal cell–derived EVs, stromal cells, or CM. After coculture, live cells were counted after trypan blue staining. For clonogenic assays, cell pellets were suspended in PBS-FCS (10%), mixed, and cultured in semisolid clonogenic medium (Methocult; M3434; STEMCELL Technologies) in nontreated 35-mm dishes. Cultures were maintained for 7 d at 37°C and 5% CO_2 before colony counting. For CD45 and LSK characterization after coculture, cells were stained either with PE-conjugated anti-CD45 or anti–Sca-1 APC-conjugated anti–c-kit antibodies (PharMingen) and a cocktail of lineage FITC-conjugated antibodies (Ter119, Mac1, Gr1, B220, CD4, and CD8) and then analyzed with an Influx 500 cell sorter.

RNA sequencing and bioinformatic analyses

RNA libraries were prepared by Fasteris Life Science. In brief, total RNA was submitted to a poly-A mRNA purification using oligodT magnetic beads. Supernatants were kept for small RNA library preparation, and poly-A–RNAs after elution from the beads were prepared according to the manufacturer's protocol (TruSeq RNA Sample Prep-Kit V2; Illumina). Transcripts were broken at 95°C in presence of zinc, and first-strand cDNA syntheses were performed using random primers. A second-strand cDNA synthesis was performed in the presence of deoxyuridine triphosphate, and after a 3′ A addition step, adapters were ligated, and an amplification by PCR was performed to generate the DNA colony template libraries. Small RNA libraries were performed according to the manufacturer's protocol (TruSeq Small RNA Library Prep kit; Illumina). After acrylamide gel purification of small RNA between 18–30 nt, single-stranded ligation of 3′ adapter and the 5′ adapter were performed before reverse transcription and PCR amplification to generate the DNA colonies template. All the samples were sequenced using 1 × 50–bp single reads high-throughput sequencing (RNA-Seq) in single lane on a HiSeq 2000 sequencing system (Illumina). RNA-Seq analysis was performed on Galaxy. For mRNA libraries, sequence reads in fastq format were aligned to the mouse genome (NCBI Assembly accession number GCA_000001635) using the Tophat2 tool (Kim et al., 2013) allowing two mismatches. The number of reads for all the features were then counted using the FeatureCounts tool (Liao et al., 2014) and normalized for each library, and then Fisher's tests were performed to compare read values between different libraries. The cufflinks tool (Trapnell et al., 2010) was also used to assemble transcripts and estimate their relative abundance in each library. For small RNA libraries, sequence reads in fatsq format were trimmed from adapter sequences and aligned to the miRbase database (release 21). The 15–36-nt reads matching the reference sequences with zero or one mismatch were retained for subsequent analysis. The numbers of reads for each miRNA were then counted using the Parse miRNA bowtie matching tool (a Galaxy tool) and FeatureCounts (Liao et al., 2014) and normalized for each library, and then Fisher's tests were performed to compare read values between different libraries. For global annotation of the libraries, we used the release GRCm38 of the noncoding RNAs of fasta reference files available in Ensembl, and the release 21 of miRNA sequences from miRBase.

Quantitative RT-PCR

Quantitative RT-PCR was performed using SYBR green technology (Roche). RNA was extracted using the NucleoSpin miRNA kit (MACHEREY-NAGEL), and cDNAs were synthesized from 200 ng of total RNA with the miScript RT kit (QIAGEN) to quantify miRNA or with the Superscript III RT kit (Invitrogen) with random primers to quantify mRNA. After reverse transcription, triplicate measurements were made on 2 µl of cDNA diluted to 1:10 in a final reaction volume of 20 µl by quantitative PCR in a 96-well optical PCR plate with a Bio-Rad machine and a SYBR green PCR mixture containing 10 µl SYBR green PCR mix (Roche), 4 µl of water, 2 µl of 10 µM for each primer, and 2 µl of the sample. U6 RNA and GAPDH were used as housekeeping genes, and the mean of ΔCt was calculated for each gene of interest. Quantitative PCRs were performed under the conditions recommended by the manufacturer, and post-run dissociation curves were generated for the analysis of amplicon species.

Apoptotic assay

18 h after contact with AFT EVs or after siRNA/mimicRNA transfection, cells were analyzed by flow cytometry. Cells were washed and resuspended in annexin buffer and stained with annexin V–FITC antibody. Before cytometer analysis (MACSQuant), 7-AAD was added to monitor cell viability.

Microarray analysis

RNAs from freshly sorted LSK cells or from LSK cells cultured with or without AFT EVs for 18 h were used to carry out gene expression microarray analysis (Affymetrix arrays, mouse gene 2.0 ST). After background correction and normalization, unsupervised analyses were first performed on the global transcriptomes. ANOVA was then performed to identify genes differentially expressed in cultured LSK cells with or without AFT EVs. The data were represented with a hierarchical clustering using Euclidean distance metric, and the lists of clustered genes enriched in the different LSK cell populations were used for GO analysis.

Statistical analysis

Statistical analyses (*t* tests) were performed with GraphPad and R softwares. Data were considered statistically significant for $P < 0.05$.

Accession numbers

The NCBI GEO accession numbers for the RNA-Seq and microarray data presented in this paper are GSE76711 and GSE94074, respectively.

Online supplemental material

Fig. S1 shows representative flow cytometry analyses of EVs. EV gating strategy, CD9, CD63, and annexin V staining are shown. These analyses revealed no contamination by microparticles and highlighted two distinct populations of EVs with different CD63 expression patterns. Expressions of CD9 and CD63 have also been investigated in the cell of origin, and mean fluorescence intensities were compared between AFT and BFC cells and between AFT and BFC EVs. Fig. S2 shows the internalization assay analyzed by flow cytometry of total BM cells cultured ex vivo in the presence of stained EVs. Fig. S3 shows the size distribution of the small RNA reads of the cell and EV libraries and the differences in the RNA-Seq profiles between the HSPC-supportive and nonsupportive cells and between EVs and their cells of origin. Fig. S4 indicates molecular networks enriched in AFT EVs, the effects of AFT EVs on Lin^{neg} cells, the impact of Peg10 and miR-451 deregulation on LSK apoptosis, and the predicted and validated targets of the four most abundant miRNAs in AFT EVs down-regulated in LSK cells after EV coculture. Table S1 indicates the list of the most represented mRNAs and miRNAs in AFT EVs and up-regulated in comparison to AFT cells and BFC EVs.

Acknowledgments

We thank Geraldine Toutirais and Ghislaine Frebourg (Institut de Biologie Paris-Seine) for electron microscopy analyses. We thank Christophe Antoniewski and Marius Van den Beek (ARTbio, Institut de Biologie Paris-Seine) for help in RNA-seq analyses. Nicole Boggetto and Griselda Wentzinger (Institut Jacques Monod, ImagoSeine Bioimaging Core Facility, Paris) are acknowledged for cell sorting experiments. We thank C. Théry for critical and constructive comments on this study and for the gift of the CD63-GFP plasmid. V. Hyenne is acknowledged for the pLKO-shSCR and -shRlaB expression vectors. We also thank Sophie Gournet (UMR 7622, Centre National de la Recherche Scientifique) for excellent photographic and drawing assistance.

This study was supported by grants from the Fondation pour la Recherche Médicale (DEQ20100318258) and from the Agence Nationale pour la Recherche/California Institute for Regenerative Medicine (ANR/CIRM 0001-02).

The authors declare no competing financial interests.

Author contributions: G. Stik, P. Charbord, T. Jaffredo, and C. Durand conceived the study and wrote the manuscript. G. Stik performed the cell culture and molecular biology experiments and analyzed the data. G. Stik, P. Charbord, and C. Durand performed the bioinformatic analyses. S. Crequit and J. Durant performed the cell culture and molecular biology experiments. L. Petit performed the cell culture and animal experiments for EV uptake assays.

Submitted: 29 January 2016
Revised: 8 February 2017
Accepted: 1 May 2017

References

Abkowitz, J.L., M.T. Persik, G.H. Shelton, R.L. Ott, J.V. Kiklevich, S.N. Catlin, and P. Guttorp. 1995. Behavior of hematopoietic stem cells in a large animal. *Proc. Natl. Acad. Sci. USA.* 92:2031–2035. http://dx.doi.org/10.1073/pnas.92.6.2031

Anzai, N., Y. Lee, B.S. Youn, S. Fukuda, Y.J. Kim, C. Mantel, M. Akashi, and H.E. Broxmeyer. 2002. C-kit associated with the transmembrane 4 superfamily proteins constitutes a functionally distinct subunit in human hematopoietic progenitors. *Blood.* 99:4413–4421. http://dx.doi.org/10.1182/blood.V99.12.4413

Baglio, S.R., K. Rooijers, D. Koppers-Lalic, F.J. Verweij, M. Pérez Lanzón, N. Zini, B. Naaijkens, F. Perut, H.W. Niessen, N. Baldini, and D.M. Pegtel. 2015. Human bone marrow- and adipose-mesenchymal stem cells secrete exosomes enriched in distinctive miRNA and tRNA species. *Stem Cell Res. Ther.* 6:127. http://dx.doi.org/10.1186/s13287-015-0116-z

Bruno, S., C. Grange, M.C. Deregibus, R.A. Calogero, S. Saviozzi, F. Collino, L. Morando, A. Busca, M. Falda, B. Bussolati, et al. 2009. Mesenchymal stem cell-derived microvesicles protect against acute tubular injury. *J. Am. Soc. Nephrol.* 20:1053–1067. http://dx.doi.org/10.1681/ASN.2008070798

Charbord, P. 2010. Bone marrow mesenchymal stem cells: Historical overview and concepts. *Hum. Gene Ther.* 21:1045–1056. http://dx.doi.org/10.1089/hum.2010.115

Charbord, P., C. Pouget, H. Binder, F. Dumont, G. Stik, P. Levy, F. Allain, C. Marchal, J. Richter, B. Uzan, et al. 2014. A systems biology approach for defining the molecular framework of the hematopoietic stem cell niche. *Cell Stem Cell.* 15:376–391. http://dx.doi.org/10.1016/j.stem.2014.06.005

Chateauvieux, S., J.L. Ichanté, B. Delorme, V. Frouin, G. Piétu, A. Langonné, N. Gallay, L. Sensebé, M.T. Martin, K.A. Moore, and P. Charbord. 2007. Molecular profile of mouse stromal mesenchymal stem cells. *Physiol. Genomics.* 29:128–138. http://dx.doi.org/10.1152/physiolgenomics.00197.2006

Collino, F., M.C. Deregibus, S. Bruno, L. Sterpone, G. Aghemo, L. Viltono, C. Tetta, and G. Camussi. 2010. Microvesicles derived from adult human bone marrow and tissue specific mesenchymal stem cells shuttle selected pattern of miRNAs. *PLoS One.* 5:e11803. http://dx.doi.org/10.1371/journal.pone.0011803

Colombo, M., G. Raposo, and C. Théry. 2014. Biogenesis, secretion, and intercellular interactions of exosomes and other extracellular vesicles. *Annu. Rev. Cell Dev. Biol.* 30:255–289. http://dx.doi.org/10.1146/annurev-cellbio-101512-122326

De Luca, L., S. Trino, I. Laurenzana, V. Simeon, G. Calice, S. Raimondo, M. Podestà, M. Santodirocco, L. Di Mauro, F. La Rocca, et al. 2016. MiRNAs and piRNAs from bone marrow mesenchymal stem cell extracellular vesicles induce cell survival and inhibit cell differentiation of cord blood hematopoietic stem cells: a new insight in transplantation. *Oncotarget.* 7:6676–6692.

Du, J., S. Liu, J. He, X. Liu, Y. Qu, W. Yan, J. Fan, R. Li, H. Xi, W. Fu, et al. 2015. MicroRNA-451 regulates stemness of side population cells via PI3K/Akt/mTOR signaling pathway in multiple myeloma. *Oncotarget.* 6:14993–15007. http://dx.doi.org/10.18632/oncotarget.3802

Durand, C., C. Robin, K. Bollerot, M.H. Baron, K. Ottersbach, and E. Dzierzak. 2007. Embryonic stromal clones reveal developmental regulators of definitive hematopoietic stem cells. *Proc. Natl. Acad. Sci. USA.* 104:20838–20843. http://dx.doi.org/10.1073/pnas.0706923105

Ekström, K., H. Valadi, M. Sjöstrand, C. Malmhäll, A. Bossios, M. Eldh, and J. Lötvall. 2012. Characterization of mRNA and microRNA in human mast cell-derived exosomes and their transfer to other mast cells and blood CD34 progenitor cells. *J. Extracell. Vesicles.* 1:18389. http://dx.doi.org/10.3402/jev.v1i0.18389

Götz, R., S. Wiese, S. Takayama, G.C. Camarero, W. Rossoll, U. Schweizer, J. Troppmair, S. Jablonka, B. Holtmann, J.C. Reed, et al. 2005. Bag1 is essential for differentiation and survival of hematopoietic and neuronal cells. *Nat. Neurosci.* 8:1169–1178. http://dx.doi.org/10.1038/nn1524

Hackney, J.A., P. Charbord, B.P. Brunk, C.J. Stoeckert, I.R. Lemischka, and K.A. Moore. 2002. A molecular profile of a hematopoietic stem cell niche. *Proc. Natl. Acad. Sci. USA*. 99:13061–13066. http://dx.doi.org/10.1073/pnas.192124499

Hoshino, A., B. Costa-Silva, T.L. Shen, G. Rodrigues, A. Hashimoto, M. Tesic Mark, H. Molina, S. Kohsaka, A. Di Giannatale, S. Ceder, et al. 2015. Tumour exosome integrins determine organotropic metastasis. *Nature.* 527:329–335. http://dx.doi.org/10.1038/nature15756

Hyenne, V., A. Apaydin, D. Rodriguez, C. Spiegelhalter, S. Hoff-Yoessle, M. Diem, S. Tak, O. Lefebvre, Y. Schwab, J.G. Goetz, and M. Labouesse. 2015. RAL-1 controls multivesicular body biogenesis and exosome secretion. *J. Cell Biol.* 211:27–37. http://dx.doi.org/10.1083/jcb.201504136

Kim, D., G. Pertea, C. Trapnell, H. Pimentel, R. Kelley, and S.L. Salzberg. 2013. TopHat2: accurate alignment of transcriptomes in the presence of insertions, deletions and gene fusions. *Genome Biol.* 14:R36. http://dx.doi.org/10.1186/gb-2013-14-4-r36

Liao, Y., G.K. Smyth, and W. Shi. 2014. featureCounts: an efficient general purpose program for assigning sequence reads to genomic features. *Bioinformatics.* 30:923–930. http://dx.doi.org/10.1093/bioinformatics/btt656

Lim, M., Y. Pang, S. Ma, S. Hao, H. Shi, Y. Zheng, C. Hua, X. Gu, F. Yang, W. Yuan, and T. Cheng. 2016. Altered mesenchymal niche cells impede generation of normal hematopoietic progenitor cells in leukemic bone marrow. *Leukemia*. 30:154–162. http://dx.doi.org/10.1038/leu.2015.210

Luo, M., M. Jeong, D. Sun, H.J. Park, B.A. Rodriguez, Z. Xia, L. Yang, X. Zhang, K. Sheng, G.J. Darlington, et al. 2015. Long non-coding RNAs control hematopoietic stem cell function. *Cell Stem Cell.* 16:426–438. http://dx.doi.org/10.1016/j.stem.2015.02.002

Mittelbrunn, M., C. Gutiérrez-Vázquez, C. Villarroya-Beltri, S. González, F. Sánchez-Cabo, M.A. González, A. Bernad, and F. Sánchez-Madrid. 2011. Unidirectional transfer of microRNA-loaded exosomes from T cells to antigen-presenting cells. *Nat. Commun.* 2:282. http://dx.doi.org/10.1038/ncomms1285

Moore, K.A., H. Ema, and I.R. Lemischka. 1997. In vitro maintenance of highly purified, transplantable hematopoietic stem cells. *Blood.* 89:4337–4347.

Morelli, A.E., A.T. Larregina, W.J. Shufesky, M.L. Sullivan, D.B. Stolz, G.D. Papworth, A.F. Zahorchak, A.J. Logar, Z. Wang, S.C. Watkins, et al. 2004. Endocytosis, intracellular sorting, and processing of exosomes by dendritic cells. *Blood.* 104:3257–3266. http://dx.doi.org/10.1182/blood-2004-03-0824

Morrison, S.J., and D.T. Scadden. 2014. The bone marrow niche for haematopoietic stem cells. *Nature.* 505:327–334. http://dx.doi.org/10.1038/nature12984

Mulcahy, L.A., R.C. Pink, and D.R. Carter. 2014. Routes and mechanisms of extracellular vesicle uptake. *J. Extracell. Vesicles.* 3:24641. http://dx.doi.org/10.3402/jev.v3.24641

Nolta, J.A., F.T. Thiemann, J. Arakawa-Hoyt, M.A. Dao, L.W. Barsky, K.A. Moore, I.R. Lemischka, and G.M. Crooks. 2002. The AFT024 stromal cell line supports long-term ex vivo maintenance of engrafting multipotent human hematopoietic progenitors. *Leukemia.* 16:352–361. http://dx.doi.org/10.1038/sj.leu.2402371

Nolte-'t Hoen, E.N.M., H.P.J. Buermans, M. Waasdorp, W. Stoorvogel, M.H.M. Wauben, and P.A.C. 't Hoen. 2012. Deep sequencing of RNA from immune cell-derived vesicles uncovers the selective incorporation of small non-coding RNA biotypes with potential regulatory functions. *Nucleic Acids Res.* 40:9272–9285. http://dx.doi.org/10.1093/nar/gks658

Oostendorp, R.A., C. Robin, C. Steinhoff, S. Marz, R. Bräuer, U.A. Nuber, E.A. Dzierzak, and C. Peschel. 2005. Long-term maintenance of hematopoietic stem cells does not require contact with embryo-derived stromal cells in cocultures. *Stem Cells.* 23:842–851. http://dx.doi.org/10.1634/stemcells.2004-0120

Pefanis, E., J. Wang, G. Rothschild, J. Lim, D. Kazadi, J. Sun, A. Federation, J. Chao, O. Elliott, Z.P. Liu, et al. 2015. RNA exosome-regulated long non-coding RNA transcription controls super-enhancer activity. *Cell.* 161:774–789. http://dx.doi.org/10.1016/j.cell.2015.04.034

Peng, W., H. Fan, G. Wu, J. Wu, and J. Feng. 2015. Upregulation of long noncoding RNA PEG10 associates with poor prognosis in diffuse large B cell lymphoma with facilitating tumorigenicity. *Clin. Exp. Med.* 16:177–182. http://dx.doi.org/10.1007/s10238-015-0350-9

Qin, B., Y. Cao, H. Yang, B. Xiao, and Z. Lu. 2015. MicroRNA-221/222 regulate ox-LDL-induced endothelial apoptosis via Ets-1/p21 inhibition. *Mol. Cell. Biochem.* 405:115–124. http://dx.doi.org/10.1007/s11010-015-2403-5

Quesenberry, P.J., J. Aliotta, M.C. Deregibus, and G. Camussi. 2015. Role of extracellular RNA-carrying vesicles in cell differentiation and reprogramming. *Stem Cell Res. Ther.* 6:153. http://dx.doi.org/10.1186/s13287-015-0150-x

Ratajczak, J., K. Miekus, M. Kucia, J. Zhang, R. Reca, P. Dvorak, and M.Z. Ratajczak. 2006. Embryonic stem cell-derived microvesicles reprogram hematopoietic progenitors: evidence for horizontal transfer of mRNA and protein delivery. *Leukemia.* 20:847–856. http://dx.doi.org/10.1038/sj.leu.2404132

Savina, A., M. Furlán, M. Vidal, and M.I. Colombo. 2003. Exosome release is regulated by a calcium-dependent mechanism in K562 cells. *J. Biol. Chem.* 278:20083–20090. http://dx.doi.org/10.1074/jbc.M301642200

Simons, M., and G. Raposo. 2009. Exosomes—vesicular carriers for intercellular communication. *Curr. Opin. Cell Biol.* 21:575–581. http://dx.doi.org/10.1016/j.ceb.2009.03.007

Théry, C., S. Amigorena, G. Raposo, and A. Clayton. 2006. Isolation and characterization of exosomes from cell culture supernatants and biological fluids. *Curr. Protoc. Cell Biol.* 3:22. http://dx.doi.org/10.1002/0471143030

Trapnell, C., B.A. Williams, G. Pertea, A. Mortazavi, G. Kwan, M.J. van Baren, S.L. Salzberg, B.J. Wold, and L. Pachter. 2010. Transcript assembly and quantification by RNA-Seq reveals unannotated transcripts and isoform switching during cell differentiation. *Nat. Biotechnol.* 28:511–515. http://dx.doi.org/10.1038/nbt.1621

Valadi, H., K. Ekström, A. Bossios, M. Sjöstrand, J.J. Lee, and J.O. Lötvall. 2007. Exosome-mediated transfer of mRNAs and microRNAs is a novel mechanism of genetic exchange between cells. *Nat. Cell Biol.* 9:654–659. http://dx.doi.org/10.1038/ncb1596

van der Vlist, E.J., E.N. Nolte-'t Hoen, W. Stoorvogel, G.J. Arkesteijn, and M.H. Wauben. 2012. Fluorescent labeling of nano-sized vesicles released by cells and subsequent quantitative and qualitative analysis by high-resolution flow cytometry. *Nat. Protoc.* 7:1311–1326. http://dx.doi.org/10.1038/nprot.2012.065

Wen, S., M. Dooner, Y. Cheng, E. Papa, M. Del Tatto, M. Pereira, Y. Deng, L. Goldberg, J. Aliotta, D. Chatterjee, et al. 2016. Mesenchymal stromal cell-derived extracellular vesicles rescue radiation damage to murine marrow hematopoietic cells. *Leukemia.* 30:2221–2231. http://dx.doi.org/10.1038/leu.2016.107

Zhou, Y., H. Xu, W. Xu, B. Wang, H. Wu, Y. Tao, B. Zhang, M. Wang, F. Mao, Y. Yan, et al. 2013. Exosomes released by human umbilical cord mesenchymal stem cells protect against cisplatin-induced renal oxidative stress and apoptosis in vivo and in vitro. *Stem Cell Res. Ther.* 4:34. http://dx.doi.org/10.1186/scrt194